

# A comparison of [11C]-(R)PK11195 tracer kinetics and MRI-based vascularity-related parameters in gliomas

Chao Li<sup>1,2</sup>, Zhangjie Su<sup>1</sup>, Ka-Loh Li<sup>1</sup>, Alex Gerhard<sup>1</sup>, Gerard Thompson<sup>1</sup>, Xiaoping Zhu<sup>1</sup>, Rainer Hinze<sup>1</sup>, Federico Roncaroli<sup>3</sup>, Karl Herholz<sup>1</sup>, and Alan Jackson<sup>1</sup>  
<sup>1</sup>Wolfson Molecular Imaging Centre, The University of Manchester, Manchester, United Kingdom, <sup>2</sup>Department of Neurosurgery, Shanghai First People's Hospital, Shanghai, China, <sup>3</sup>“John Fulcher” Neuro-Oncology Lab, Imperial College London, London, United Kingdom

**Target audience:** Investigators using neuroimaging in glioma studies.

**Purpose:** Our previous PET study in human gliomas has shown the tracer kinetics of [11C]-(R)PK11195 and the potential to detect malignant transformation of non-enhancing gliomas<sup>1,2</sup>. The purpose of this study is to compare the MRI-based vascularity-related parametric maps to the PET-based tracer kinetics maps, and their potential to detect early malignant transformation from low-grade to higher grade gliomas, which is usually unrecognized on conventional MRI.

**Methods:** Seventeen glioma patients (eleven WHO grade II, four grade III; one grade IV, one low-grade glioma without histopathologic diagnosis) underwent structural, dynamic susceptibility contrast (DSC), high temporal resolution (HT,  $\Delta t = 3$  s) dynamic contrast-enhanced (DCE) MRI and dynamic [11C]-(R)PK11195 PET scans. The dynamic DSC and DCE were performed using specifically designed imaging protocol. High temporal resolution DSC and DCE were acquired using isotropic spatial resolution with a voxel size similar to dynamic [11C]-(R)PK11195. Parametric maps of relative cerebral blood flow (rCBF), volume (rCBV), mean transit time (MTT), and tracer delay time ( $t_d$ ) were generated from the DSC data using a commercial software MISTar (Apollo Medical Imaging Technology). The singular value decomposition (SVD) was performed. The DCE data were analyzed using a hybrid approach<sup>3</sup> based on the extended Tofts model, generating maps of the fractional plasma volume,  $v_p$ , transfer constant,  $K^{trans}$ , and the fractional volume of extravascular extracellular space,  $v_e$ , in addition to native longitudinal relaxation time ( $R_{1N}$ ) and a semi-quantitative parameter,  $rAUC_{90s}$  (the baseline-normalized area under the signal intensity (SI) curve over a time interval of 90 s). Parametric maps of [11C]-(R)PK11195 uptake, i.e. the binding potential ( $BP_{ND}$ ) and the ratio of influx ( $R_i$ ), were generated with a simplified reference tissue model<sup>4</sup>. For each subject, MRI images and parametric maps were co-registered to the summed PET image. Tumor region of interest (ROI) was first manually delineated on the co-registered T2-weighted FLAIR images and then confirmed against the T1-weighted contrast-enhanced MR image. The average and distribution of these parameters over the whole tumor volume were calculated (voxels with  $v_p > 0.3$  or  $R_{1N} \leq 0$  were excluded to avoid major vessels, calcification and other artifacts). Pearson linear regression analysis was performed to evaluate relationship between these MRI vascularity-related parameters and the [11C]-(R)PK11195 uptake.

**Results:** DCE- and DSC-MR parameters correlated with [11C]-(R)PK11195 PET parameters, both of which demonstrated significant changes in non-enhancing high-grade glioma. Figure 1 shows co-registered  $BP_{ND}$ , conventional post-contrast T1W (T1W+C), and MRI parametric maps from a patient with grade III glioma (white arrows). The tumor SI-time curve demonstrates a higher initial enhancement but a lower baseline SI compared with its mirror ROI, which was caused by tumor's lower  $R_{1N}$  (i.e., higher  $T_{1N}$ ). Although the initial contrast enhancement relative to the baseline and the blood (or plasma) volume derived from DSC or DCE MRI show higher level in the tumor ROI, the conventional T1W+C image shows minor or no enhancement within the tumor. Table 1 lists the correlations of the two PET tracer uptake parameters with MRI parameters. For most voxels within the non-enhancing gliomas,  $K^{trans}$  and  $v_e$  were not measurable with Tofts model, and not included in this table. Figure 2 shows plots of the PET based kinetic parameters, i.e.  $BP_{ND}$  and  $R_i$ , against the MRI-based vascularity-related parameters. Among them, the two most significant correlations are:  $R_i$  vs rCBF ( $r = 0.83$ ,  $p < 0.0001$ ), and  $BP_{ND}$  vs MTT ( $r = -0.74$ ,  $p = 0.0007$ ).

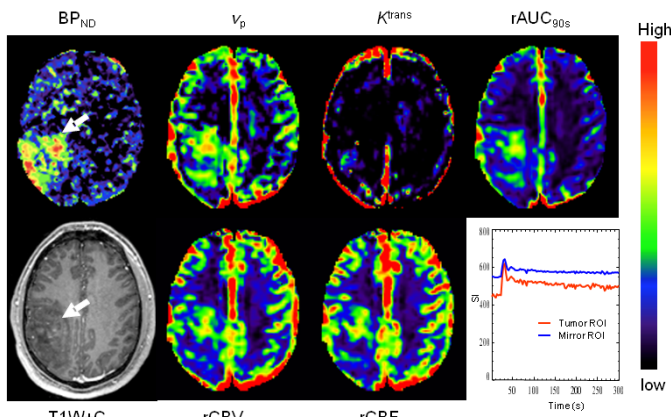


Figure 1.  $BP_{ND}$  (top left), T1W+C image (bottom left), perfusion and pharmacokinetic parametric maps. SI-time curves extracted from the ROI of the glioma and its mirror on the unaffected hemisphere were also shown (bottom right).

**Results:** DCE- and DSC-MR parameters correlated with [11C]-(R)PK11195 PET parameters, both of which demonstrated significant changes in non-enhancing high-grade glioma. Figure 1 shows co-registered  $BP_{ND}$ , conventional post-contrast T1W (T1W+C), and MRI parametric maps from a patient with grade III glioma (white arrows). The tumor SI-time curve demonstrates a higher initial enhancement but a lower baseline SI compared with its mirror ROI, which was caused by tumor's lower  $R_{1N}$  (i.e., higher  $T_{1N}$ ). Although the initial contrast enhancement relative to the baseline and the blood (or plasma) volume derived from DSC or DCE MRI show higher level in the tumor ROI, the conventional T1W+C image shows minor or no enhancement within the tumor. Table 1 lists the correlations of the two PET tracer uptake parameters with MRI parameters. For most voxels within the non-enhancing gliomas,  $K^{trans}$  and  $v_e$  were not measurable with Tofts model, and not included in this table. Figure 2 shows plots of the PET based kinetic parameters, i.e.  $BP_{ND}$  and  $R_i$ , against the MRI-based vascularity-related parameters. Among them, the two most significant correlations are:  $R_i$  vs rCBF ( $r = 0.83$ ,  $p < 0.0001$ ), and  $BP_{ND}$  vs MTT ( $r = -0.74$ ,  $p = 0.0007$ ).

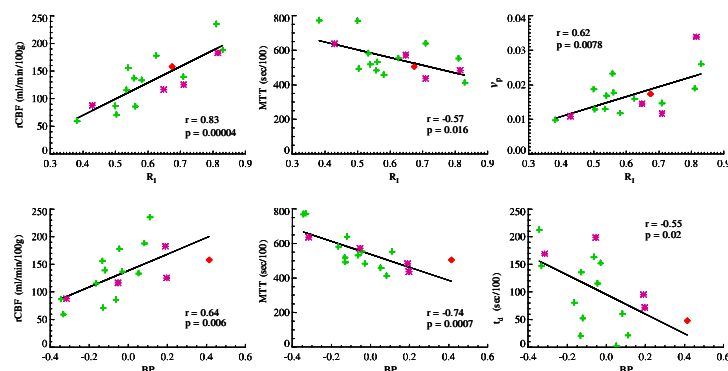


Figure 2. Top row: plots of  $R_i$  vs rCBF (left), MTT (middle),  $v_p$  (right). Bottom row: Plots of  $BP_{ND}$  vs rCBF (left), MTT (middle), and  $t_d$  (right). Symbols in place of each tumor were color rendered to represent their WHO grades, i.e. red: grade IV; purple: grade III; green: grade II, including one LGG without histopathologic diagnosis.

Table 1. Correlations between PET-based and MRI-based kinetic parameters

	rCBF	MTT	$t_d$	rCBV	$v_p$
$R_i$	$r = 0.83$ ( $p < 0.0001$ )	$r = -0.57$ ( $p = 0.02$ )	$r = -0.49$ ( $p = 0.04$ )	$r = 0.64$ ( $p = 0.006$ )	$r = 0.62$ ( $p = 0.008$ )
$BP_{ND}$	$r = 0.64$ ( $p = 0.006$ )	$r = -0.74$ ( $p = 0.0007$ )	$r = -0.55$ ( $p = 0.02$ )	$r = 0.38$ ( $p = 0.13$ )	$r = 0.41$ ( $p = 0.10$ )

**Discussions:** Immunohistochemistry in our previous studies confirmed that TSPO within gliomas was expressed mainly by neoplastic cells and correlated with [11C]-(R)PK11195 uptake of the tumor, while the contribution from tumor-infiltrating microglia was minimal<sup>1,2</sup>. The major contribution of this study is the discovery of close relationship between MRI-based perfusion parameters, rCBF, MTT,  $t_d$ ,  $v_p$ , etc, and the PET-based uptake parameters,  $BP_{ND}$  and  $R_i$ , where the change of vascularity and neuroinflammation was unrecognized on the conventional 3D contrast enhanced MRI. This finding addresses the importance of performing dynamic contrast enhanced studies, DCE or DSC, rather than the conventional 3D T1W+C, which has only a single time frame, in the characterization of the vascularity changes of tumors, thus probably

reflecting the status of malignant transformation of gliomas. In conclusion, a combination of advanced MRI and PET techniques could provide more information about the nature of the tumor, which would be useful in planning of targeted biopsy, surgical resection, and radiation therapy.

## References:

- Su et al, Eur J Nucl Med Mol Imaging. 2013; 40:1406–1419.
- Su et al. Mol Imaging Biol. 2012; 14 (suppl 2): s2087.
- Li and Jackson, MRM. 2003; 50:1286.
- Lammertsma and Hume. NeuroImage. 1996; 4:153-158.

**Acknowledgements:** Supported by INMiND.